RESEARCH ARTICLE
SPACE PHYSICS: IONOSPHERIC PHYSICS

Earth and Planetary Physics
4: 588–597, 2020
doi: 10.26464/epp2020068

Evidence of X-mode heating suppressing O-mode heating

Ting Feng, Chen Zhou*, Xiang Wang, MoRan Liu*, and ZhengYu Zhao

Department of Space Physics, School of Electronic Information, Wuhan University, Wuhan 430072, China

Key Points:

- X-mode heating suppresses O-mode heating owing to the electron temperature enhancement
- Overshoot occurs in cold-start O-mode heating, which is different from X-mode heating
- The electron temperature is negatively correlated with the growth rate of thermal parametric instability

Citation: Feng, T., Zhou, C., Wang, X., Liu, M. R. and Zhao, Z. Y. (2020). Evidence of X-mode heating suppressing O-mode heating. *Earth Planet. Phys.*, *4*(6), 588–597. http://doi.org/10.26464/epp2020068

Abstract: In this study, we present three experiments carried out at the EISCAT (European Incoherent Scatter Scientific Association) heating facility on October 29 and 30, 2015. The results from the first experiment showed overshoot during the O-mode heating period. The second experiment, which used cold-start X-mode heating, showed the generation of parametric decay instability, whereas overshoot was not observed. The third experiment used power-stepped X-mode heating with noticeable O-mode wave leakage. Parametric decay instability and oscillating two-stream instability were generated at the O-mode reflection height without the overshoot effect, which implies suppression of the thermal parametric instability with X-mode heating. We propose that the electron temperature increased because X-mode heating below the upper hybrid height decreased the growth rate of the thermal parametric instability.

Keywords: ionospheric heating; parametric decay instability; thermal parametric instability; overshoot; suppression

1. Introduction

Parametric instability is the most important physical process in ionospheric heating. Phenomena such as high-frequency enhanced ion lines (HFILs), high-frequency enhanced plasma lines (HFPLs), and stimulated electromagnetic emissions (SEEs; Stubbe et al., 1984) are strongly connected to parametric decay instability (PDI) (Perkins et al., 1974; Fejer, 1979; Robinson, 1983; Kuo, 2015), oscillating two-stream instability (OTSI; Kuo et al., 1997; Kuo, 2015), thermal parametric instability (TPI; Lee and Kuo, 1983; Kuo, 2015), and related physical processes.

Parametric decay instability, OTSI, and TPI can usually be generated by an O-mode polarized pump wave with the electric field in excess of the instability threshold. Parametric decay instability is a typical three-wave coupling process in which the pump wave interacts with two electrostatic waves, Langmuir waves and an ion acoustic wave, which are induced by the ponderomotive force near the ordinary pump wave (O-mode) reflection altitude (Fejer, 1979; Kuo, 2015). In PDI theory, the ion acoustic wave is induced only when Langmuir waves exist (Stubbe et al., 1992). Oscillating two-stream instability occurs when a pump wave decays into two Langmuir waves and a zero-frequency periodic structure (a purely growing mode) near the O-mode reflection height (Stubbe et al., 1992; Kuo et al., 1997; Kuo, 2015). The difference between PDI and OTSI lies in the fact that the HFPLs of PDI have a frequency offset from the pump wave, whereas the HFPLs of OTSI have a zero-frequency offset from the heater wave (Kuo et al., 1997; Bryers et al., 2013). Meter-scale field-aligned irregularities (FAIs) are produced by TPI at the upper hybrid (UH) resonance region (Vas'kov and Gurevich, 1975; Frolov et al., 1999; Bryers et al, 2013), which is a few kilometers lower than the reflection height of an O-mode pump wave (Kuo, 2015). The high-frequency sidebands of PDI and OTSI are propagating Langmuir waves, whereas the high-frequency sidebands of TPI are propagating UH waves, which cannot be directly detected by ultra high frequency (UHF) or very high frequency radar (Kuo et al., 1997).

Competition between TPI and PDI in high-frequency ionospheric heating has been investigated for many years. A general feature of the competition between TPI and PDI in O-mode pump wave heating is "overshoot," particularly for a cold-start heating experiment. The strong impact of the UH instability associated with the FAIs can result in suppression of the Langmuir turbulence at the reflection height (Thidé et al., 2005; Kuo, 2014). Overshoot occurs after a cold start (which has an off period of a few seconds) of the heating transmitter in a normal O-mode pump wave experiment (Fejer, 1979) and behaves as if there is an unusually rapid rise in the measured electron temperature (Showen and Kim, 1978). Parametric decay instability saturates within milliseconds, whereas the formation of small-scale FAIs saturates within several hundreds of milliseconds (Inhester et al., 1981); therefore, the overshoot appears and lasts for a few seconds before the intensity falls to a lower level (Showen and Kim, 1978). Fejer (1979) theorized that the structures of striations associated with TPI affect the over-

Correspondence to: C. Zhou, chenzhou@whu.edu.cn
M. R. Liu, moranliu@whu.edu.cn
Received 06 JUN 2020; Accepted 10 AUG 2020.
Accepted article online 03 SEP 2020.

shoot in the O-mode pump experiment. Bryers et al. (2013) also reported that striations generated by TPI caused anomalous absorption of the pump wave and consequently decreased the HFPL and HFIL amplitudes.

For the extraordinary radio wave (X-mode) heating experiments, it is generally accepted that both Langmuir parametric instabilities (PDI and OTSI) and TPI cannot be excited. This is because (1) X-mode pump waves do not have a strong enough parallel electric field at the X-mode reflection height and (2) the frequency matching condition is not satisfied at the X-mode reflection height. It is surprising that HFPLs and HFILs resulting from X-mode pumping have been directly observed in recent X-mode heating experiments (Blagoveshchenskaya et al., 2014, 2015, 2017; Wang X et al., 2016a, b; Wang X and Zhou C, 2017). Optical emissions (Blagoveshchenskaya et al., 2014), artificial small-scale FAIs (Blagoveshchenskaya et al., 2011, 2013), narrow SEEs (Blagoveshchenskaya et al., 2015, 2017), HFILs, and HFPLs (Blagoveshchenskaya et al., 2014, 2015, 2017; Wang X et al., 2016b; Wang X and Zhou C, 2017) have been observed during these recent X-mode heating experiments. Vas'kov and Ryabova (1998) reported that the UH waves can also be excited by X-mode heating through PDI near the reflection height. Blagoveshchenskaya et al. (2014) indicated that under the X-mode heating condition, PDI is not quenched and coexists with FAIs, unlike the examples for O-mode heating (Blagoveshchenskaya et al., 2014). Frolov et al. (1999), using the Sura Ionospheric Heating Facility (Vasilsursk, Russia), proposed that X-mode heating suppresses the generation of high-frequency plasma turbulence caused by O-mode heating.

In this study, we report a unique experiment using the EISCAT UHF radar in Tromsø, Norway. The experiment shows the non-quenched feature of PDI from O-mode heating as resulting from the simultaneous effects of X-mode ohmic heating. Unlike previous research studies, we investigated the competition of PDI with TPI by taking advantage of concurrent O-mode and X-mode heating. In addition, we gained insight into the suppression mechanism of TPI in X-mode heating by examining O-mode wave leakage.

The outline of this article is as follows: Section 2 presents a brief introduction of the experimental facility and the experimental data. In Section 3, we first present a typical overshoot PDI experiment by O-mode heating at EISCAT. We then show two examples of power-stepped X-mode heating experiments on October 29, 2015, and October 30, 2015. The spectral variations in the enhanced plasma lines and ion lines observed by EISCAT are given. We interpret these instabilities as being caused by the reflection heights of the O-mode and X-mode. Third, we analyze the spectra of the ion and plasma lines with different pump wave powers. Further discussion of the observations and theoretical calculations is presented in Section 4, followed by a short summary in Section 5.

2. Data

We present incoherent scatter radar observations with a time resolution of 5 s and height resolution of 3 km that were obtained in three modified ionospheric experiments. The experiments were performed by the Russian team led by N. F. Blagoveshchenskaya, and the effective radiated power (ERP) in plots of the beam pattern was calculated by software written by Andrew Senior (https://www.eiscat.uit.no/DataBases/). The first experiment was O-mode wave heating with power stepping between 13:12 and 13:28 universal time (UT) on October 29, 2015. In this experiment, the incident wave along the magnetic field in ordinary mode was operated at f_0 = 7.953 MHz and with a duty cycle of 2 min on and 1 min off. The power-stepping ERPs were 4.8, 13.7, 48.6, 138.8, and 289.4 MW. The second experiment was X-mode wave power-stepped heating between 13:31 and 14:01 UT on October 29, 2015. This experiment had a heating frequency of f_0 = 7.953 MHz, a duty cycle of 2 min on and 1 min off, and increasing power for each subsequent pulse. The ERPs in this case were 0, 0, 5.5, 46.5, 85.1, 112.2, 141, 294, 435.8, and 523.2 MW. The third experiment also concerned X-mode wave heating power-stepping between 10:30 and 10:50 UT on October 30, 2015. In this experiment, the incident wave along the magnetic field in extraordinary mode was operated at f_0 = 7.1 MHz, with ERPs of 34.8, 83.7, 168.8, 250.7, 334.6, 337.3, 240.1, 168.2, 85.4, and 34.7 MW, which was changed every 2 min.

The HFILs and HFPLs were analyzed by the EISCAT Real Time Graph from the EISCAT website (https://www.eiscat.se/rtg/remtg.html), and the temporal–altitude variation of the background plasma parameters was calculated by using Grand Unified Incoherent Scatter Design and Analysis Package software (GUISDAP; Lehtinen and Huuskonen, 1996). All data were obtained with the EISCAT UHF radar, which can detect parallel Langmuir waves and ion acoustic waves, both of which lead directly to parametric instability stimulated by a high-frequency pump wave (Wang X et al., 2016b). The ion lines and plasma lines indicate the backscatter from the ion acoustic waves and Langmuir waves, respectively. In addition, because of technical limitations of the UHF radar, only the downshifted plasma lines could be measured (Senior et al., 2013).

3. Results

The results of the first experiment (Figure 1) illustrate ionospheric features modified by a typical O-mode pump wave. Figure 1a shows the temporal variation in ERP. Figure 1b shows the UHF radar undecoded spectra of downshifted plasma lines versus time at an altitude of ~219.1 km. Figure 1c shows the temporal–altitude behavior of the spectra of the downshifted plasma line at 7.96 MHz. The plasma lines at −7.96 MHz at 219.1 km for the entire cycle are presented in Figure 1d. As shown in Figure 1a–1c, the ERP increases with time and the plasma lines are enhanced at −7.96 MHz, which suggests the generation of PDI. Panel 1d shows a typical feature of an O-mode pump wave in which an overshoot phenomenon disappears soon after the pump-on status, which indicates the quenching of PDI. We can also observe overshoot after every cold start even when the ERP is small (e.g. 4.8 MW), as shown in Figure 1d. After overshoot, the power of the plasma lines reduces to a steady-state level, which still fluctuates (Showen and Kim, 1978).

Figure 2 shows the behavior of the plasma lines observed from the second experiment. Figure 2a shows the temporal variation in

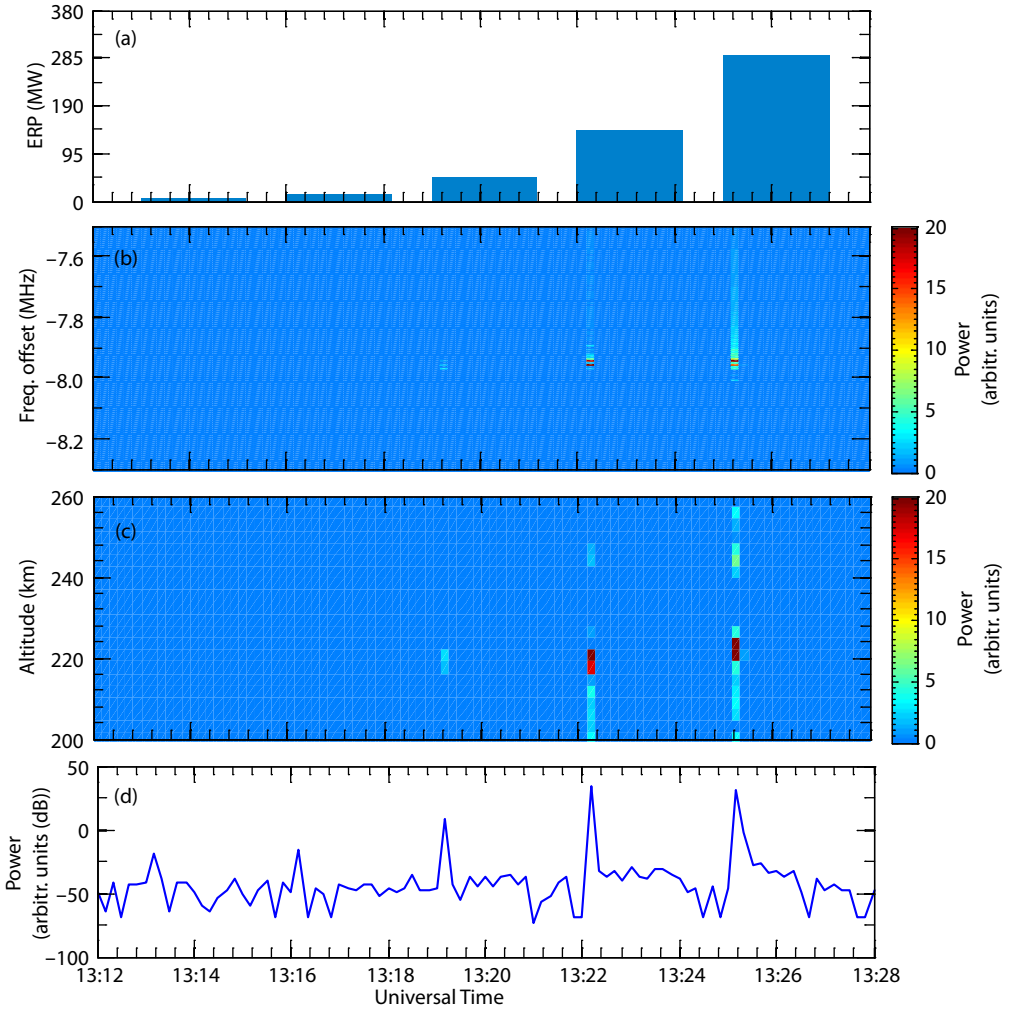

Figure 1. Plasma lines observed by the EISCAT ultra high frequency (UHF) radar during the power-stepped O-mode ionospheric heating experiment with a pump wave frequency of f_0 = 7.953 MHz between 13:12 and 13:28 UT on October 29, 2015. (a) Temporal variation in the effective radiated power (ERP), 4.8, 13.7, 48.6, 138.8, and 289.4 MW; (b) the UHF radar undecoded spectra of downshifted plasma lines versus time at ~219.1 km; (c) temporal–altitude behavior of the spectra of the downshifted plasma lines at about −7.96 MHz; (d) plasma lines at −7.96 MHz at 219.1 km during the entire cycle.

the ERP. Figure 2b is the UHF radar undecoded spectra of the downshifted plasma lines versus time over the altitude range of ~222 to ~225 km. Figure 2c shows the temporal–altitude behavior of spectra of the downshifted plasma lines at around −7.96 MHz. The plasma lines at −7.96 MHz at 225 km over the entire cycle are presented in Figure 2d. Additionally, the leakage from the X-mode to the O-mode in this experiment was negligible: less than 1% of the full ERP was able to leak to the O-mode. Bryers et al. (2013) observed that the artificial ionospheric turbulence generated in high-frequency wave heating depends on the power of the pump wave. Stubbe et al. (1992) also proposed that the amplitudes of HFILs and HFPLs are enhanced with an increase in input power. In Figure 2b and 2c, PDI exists only for the three highest pump powers (294.0, 435.8, and 523.2 MW) at the X-mode reflection altitude. Parametric decay instability is not quenched and persists during the pump-on cycle. By comparison with the O-mode heating in the first experiment, we see that overshoot does not occur in the X-mode heating under the same cold-start condition. This result suggests the suppression of TPI in X-mode heating.

The results of the third experiment are shown in Figures 3–6. Because of the leakage problem of the antenna, pump waves with both O-mode and X-mode polarization were transmitted simultaneously. According to EISCAT UHF observations, we were able to distinguish PDI generated by the O-mode from the X-mode by carefully identifying the heights of the HFIL and HFPL spectra. The reflection height of the O-mode heating wave was calculated by $\omega_0^2 = \omega_p^2$, where ω_0 is the pump wave frequency and ω_p is the local plasma frequency. The X-mode reflects when

$$\omega_p^2 = \omega_0 (\omega_0 - \omega_{ce}) \cos\alpha,$$

where ω_{ce} is the electron gyrofrequency and $\alpha = 12^\circ$ is the complement of the local dip angle at Tromsø, Norway. The UH resonance height is where the UH frequency ω_u is equal to that of the pump wave: $\omega_u^2 = \omega_0^2 = \omega_{ce}^2 + \omega_p^2$ (Bryers et al., 2013). Further, the relation between plasma frequency and electron density n_e is $\omega_p^2 = e^2 n_e / \varepsilon_0 m_e$, where ε_0 is the permittivity of free space and m_e is the electron mass. The corresponding reflection altitudes can be

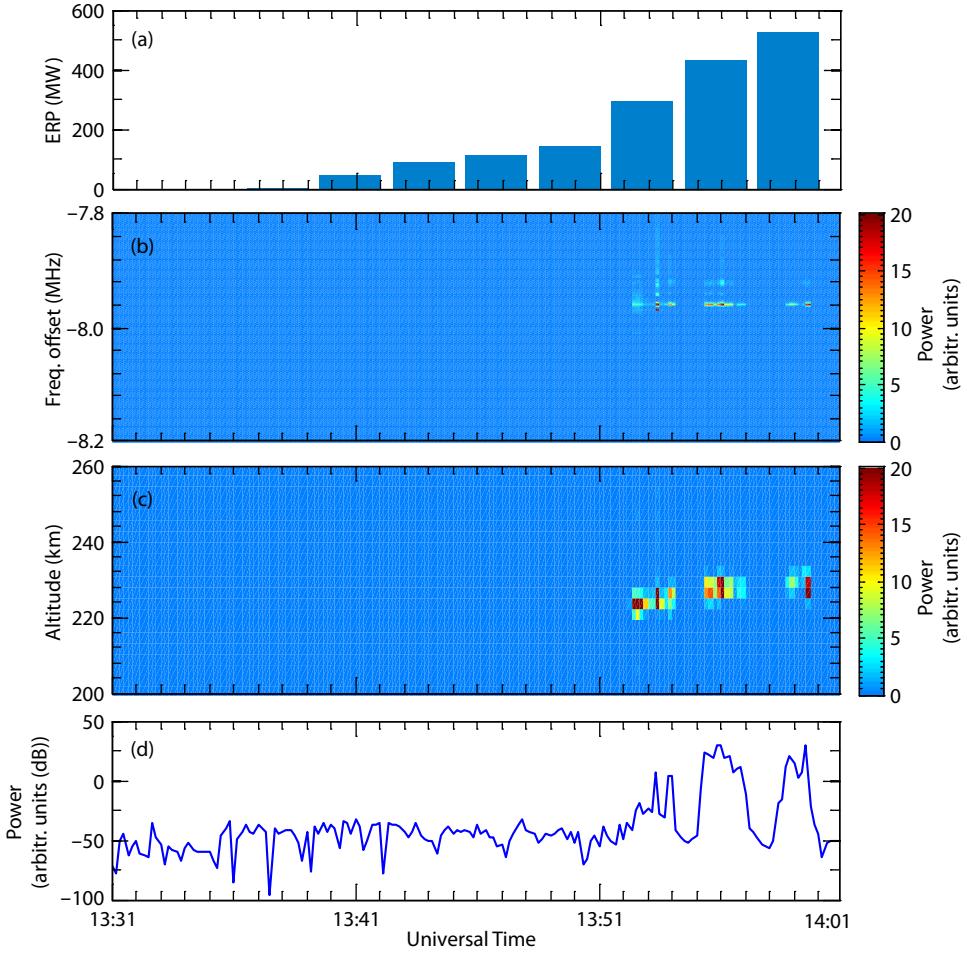

Figure 2. Plasma lines observed by the EISCAT UHF radar during the power-stepped X-mode ionospheric heating experiment with a pump wave frequency of f_0 = 7.953 MHz between 13:31 and 14:01 UT on October 29, 2015. (a) Temporal variation of the ERP, 0, 0, 5.5, 46.5, 85.1, 112.2, 141, 294, 435.8, and 523.2 MW; (b) the UHF radar undecoded spectra of downshifted plasma lines versus time in the altitude range of ~222 to ~225 km; (c) temporal–altitude behavior of the spectra of the downshifted plasma line at about −7.96 MHz; (d) plasma lines at −7.96 MHz at 225 km during the entire cycle.

obtained by estimating the electron density. In this experiment, the reflection altitudes of the O-mode wave, the X-mode wave, and the UH resonance altitude were ~224.00, ~203.84, and ~221.00 km, respectively.

Figures 3 and 4 present the HFILs and HFPLs excited by the leakage of the O-mode heating wave from the X-mode heating experiment with the EISCAT UHF radar. The transmitted ERP of the O-mode and X-mode pump waves can be found on the EISCAT website (https://www.eiscat.uit.no/DataBases/). Figures 3a and 4a show the heating ERP of the X-mode pump wave (blue line) and the corresponding O-mode wave (red line) during the entire heating experiment. In this case, at least 7.0%–8.8% ERP of the X-mode leaked to the O-mode. Figure 3b presents the temporal variations in the HFIL spectra. Figures 3c–3e are temporal–altitude behaviors of the spectra for upshifted, zero-frequency, and downshifted offset ion lines, respectively. As shown in Figures 3b–3e, the HFILs appear at three different frequencies: +10.71, 0, and −10.71 kHz, corresponding to the upshifted, zero-frequency, and downshifted ion lines, respectively. The ion line spectrum with double humps, referred to as shoulders, can be observed where the ion acoustic waves propagate toward and away from the radar. The shoulders formed during PDI can be seen in Figure 3b. The HFILs at +10.71 kHz (Figure 3c) and −10.71 kHz (Figure 3e) offset at the O-mode reflection height were also obtained. In Figure 3d, we can see that the zero-frequency offset at the O-mode reflection altitude, caused by the nonpropagating periodic structure, is a typical feature of the OTSI.

Figure 4b shows the temporal variations in the HFPL spectra. Figure 4c presents the temporal–altitude behavior of the spectra of the downshifted offset plasma lines. In Figure 4d, the power spectra are calculated from the so-called "raw electron density" data, thus showing the distribution of backscattered power of the HFILs or HFPLs in the frequency band corresponding to the ion acoustic or Langmuir wave (Blagoveshchenskaya et al., 2014). Figure 4e presents plasma lines at −7.09 MHz at 219.1 km during the entire heating period in which the overshoot effect has not been observed. During this heating period, the heating is overly dense. The pump frequency is below the critical frequencies of the O-mode wave (f_oF_2) and the X-mode wave (f_xF_2) at the F_2 layer, as shown in Figure 4f, and the data are from the EISCAT

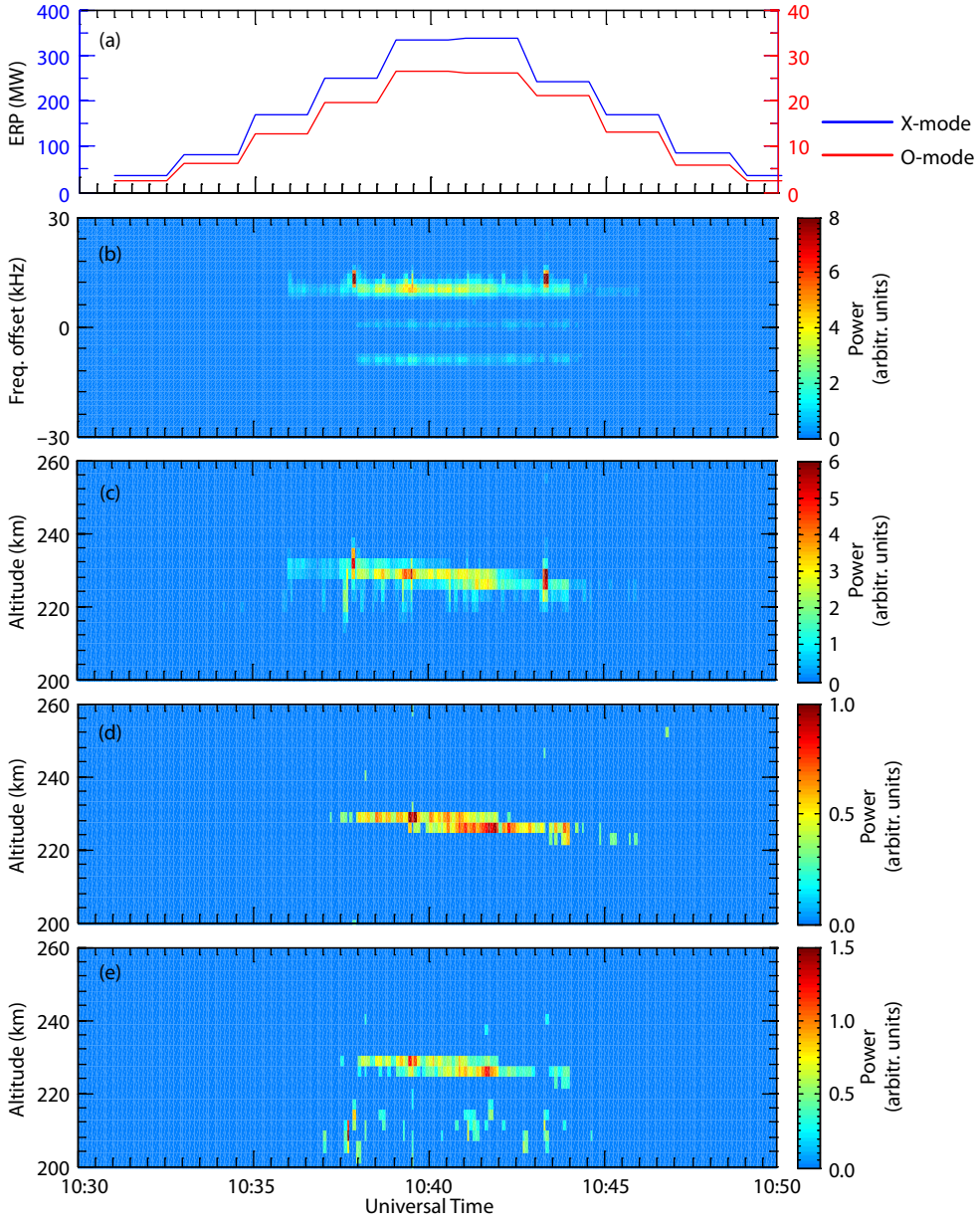

Figure 3. Ion lines observed by the EISCAT UHF radar during the power-stepped X-mode ionospheric heating experiment between 10:30 and 10:50 UT on October 30, 2015. (a) Temporal variation of ERP of the X-mode (blue) and O-mode (red); (b) temporal variations of the radio-induced ion line in the altitude range of ~224.35 to ~230.16 km; (c) temporal–altitude behavior of the spectra of the upshifted ion line at +10.71 kHz; (d) temporal–altitude behavior of the spectra of the zero-frequency offset ion line; (e) temporal–altitude behavior of the spectra of the downshifted ion line at −10.71 kHz.

Dynasonde website (https://dynserv.eiscat.uit.no/).

To exhibit the spectra for different ERP, Figures 5 and 6 provide an overview of the UHF radar spectra of the ion lines and plasma lines, respectively, for every 2 min (first 5 s of integration time) after the beginning of the pump cycle. These spectra are typical features of the PDI and OTSI induced by an O-mode pump wave. The spectra of these two figures were obtained at an O-mode reflection altitude of ~224 km. When the OTSI exists, we can see the spectra of the ion lines at a zero-frequency offset (Bryers et al., 2013). Figure 5d exhibits less pronounced spectra of the ion line shoulders without a central peak at a 0 kHz offset from the radar frequency, indicating the excitation of PDI. Figure 5e–5i shows an enhanced central peak attributable to OTSI and two intense ion line shoulders resulting from PDI (Stubbe, 1996). As the ERP of the pump wave increased, the enhanced shoulders and central peak became clearer. In Figure 5d–5h, the upshifted ion lines are enhanced preferentially to the downshifted ones because of the decay in the reflected radio wave or the cascade process (Bryers et al., 2013). In Figure 6c–6g, the enhanced plasma lines have an offset of ~0.01 MHz from the heater frequency, which is consistent with the frequency matching condition, as shown below. These features indicate that PDI and OTSI exist at the same time in the absence of TPI, and further analysis is presented in the Discussion section. Additionally, the ratio of the OTSI to PDI is independent of

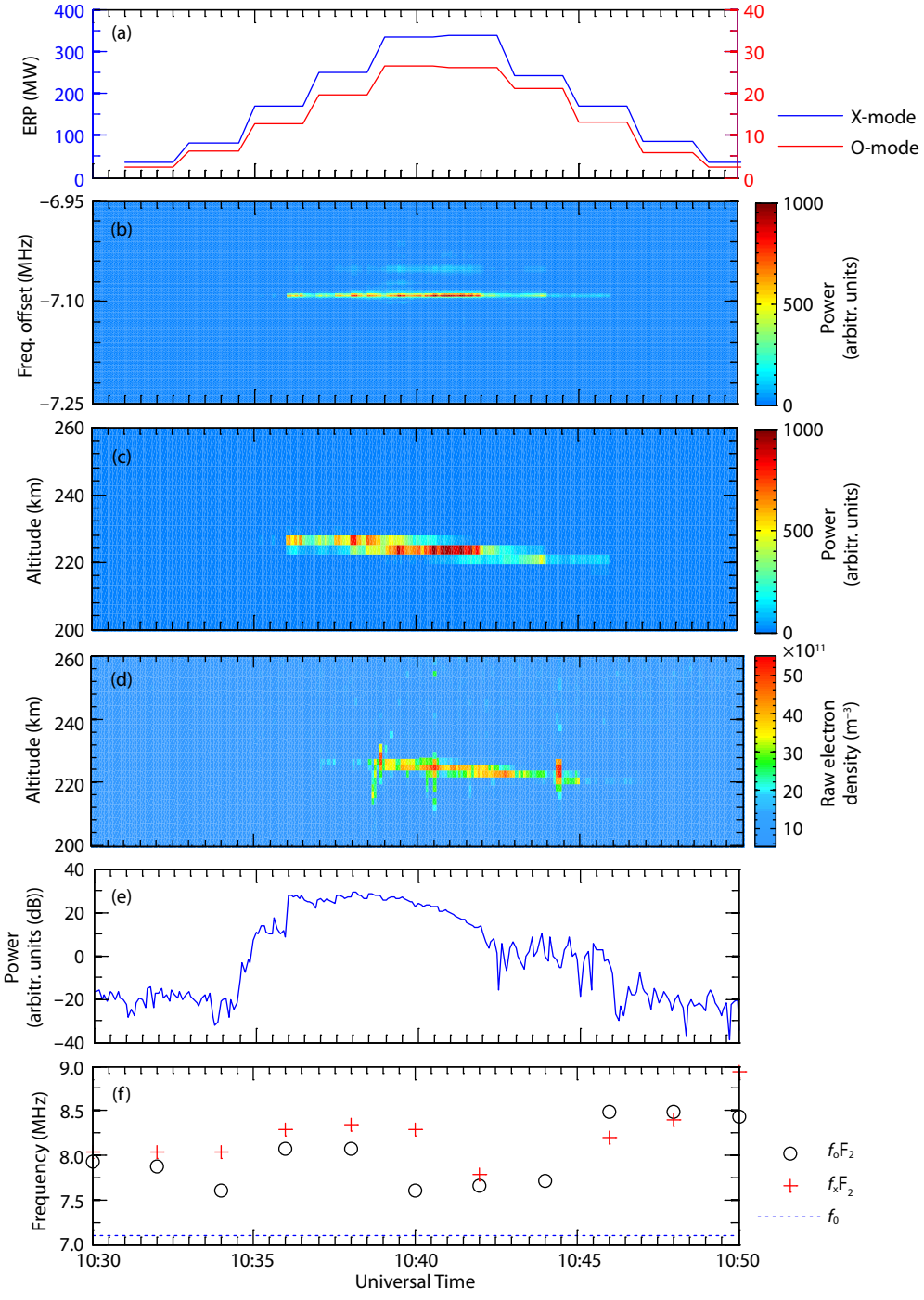

Figure 4. Plasma lines observed by the EISCAT UHF radar during the power-stepped X-mode ionospheric heating experiment with a pump wave frequency of f_0 = 7.1 MHz between 10:30 and 10:50 UT on October 30, 2015. (a) Temporal variation of ERP of the X-mode (blue) and O-mode (red); (b) the UHF radar undecoded spectra of the downshifted plasma lines versus time in the altitude range of ~219.10 to ~224.96 km; (c) temporal–altitude behavior of the spectra of the downshifted plasma line at about −7.09 MHz; (d) temporal–altitude behavior of the backscattered power (raw electron density); (e) plasma lines at −7.09 MHz at 224.96 km during the entire cycle; (f) temporal variation of the heater wave frequency (blue dashed line) and the critical frequencies of the O-mode wave (f_oF_2, red plus) and X-mode wave (f_xF_2, black circle) at the F_2 layer.

the input heater power (Kuo et al., 1997).

4. Discussion

The three-wave coupling relationship of PDI is as follows: the matching condition of OTSI is explained by Kuo (2015), and the height of FAIs generated in TPI is close to the UH resonance altitude, where the pump wave is equal to the UH resonance frequency (Blagoveshchenskaya et al., 2011; Bryers et al., 2013); thus, we have Equations (1), (2), and (3):

For PDI:

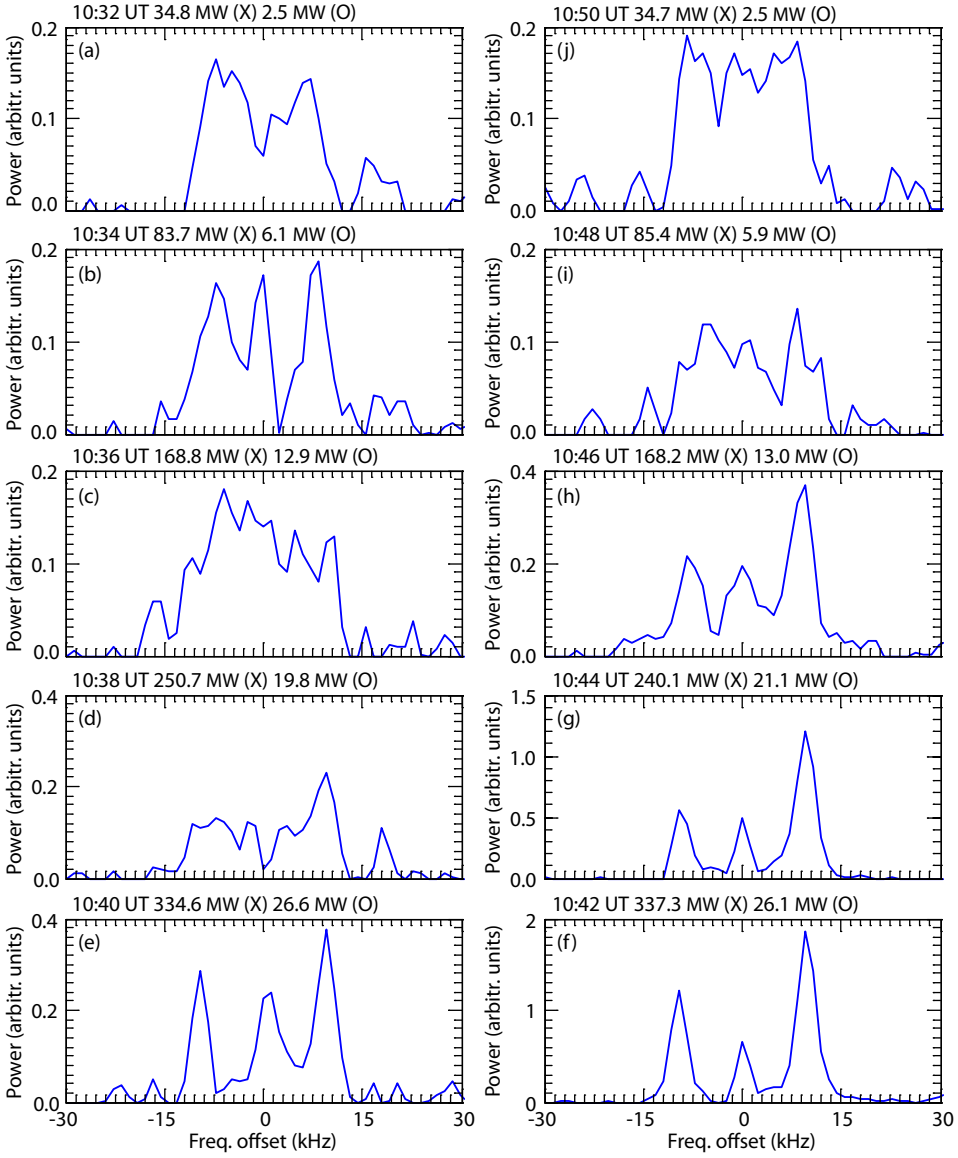

Figure 5. Ion line spectra obtained at a fixed altitude of 224.3 km with a pump wave frequency of f_0 = 7.1 MHz between 10:30 and 10:50 UT on October 30, 2015.

$$\omega_0 = \omega_{LW} + \Delta\omega_{IAW}, \tag{1}$$

For OTSI:

$$\omega_0 = \mathrm{Re}\left(\omega_{LW}\right) = \mathrm{Re}\left(\omega'_{LW}\right), \tag{2}$$

For TPI:

$$\omega_0^2 = \omega_u^2 = \omega_{ce}^2 + \omega_p^2, \tag{3}$$

where ω_{LW} and ω'_{LW} are the wave frequencies of the Langmuir waves; ω_{IAW} is the ion acoustic wave frequency. Figures 5 and 6 illustrate the consistency with Equations (1) and (2). In Figure 5, the shoulders of the ion line are at −10.71 and +10.71 kHz; in Figure 6, the peak of the plasma line is at −7.09 MHz, which add up to the pump wave frequency of 7.1 MHz.

As shown in Figure 5, the enhanced ion line shoulders and central peak coexist between 10:40 and 10:46 UT, which suggests OTSI. In Figure 6, for the heating time between 10:36 and 10:44 UT, the plasma line spectra have a frequency offset from the heating frequency, which implies the generation of a PDI. This is consistent with the conclusion by Bryers et al. (2013) that the threshold of the OTSI process is higher than that of the PDI process. The coexistence of PDI and OTSI shown in these figures is evidence of the absence of a TPI. In other words, a TPI could be induced in this condition but was suppressed by X-mode heating; at the same time, PDI and OTSI developed because of power leaking to the O-mode.

Note that the influence we describe here, which results from the leakage problem, is different from the modification of effects accomplished by additional X-mode heating to the powerful O-mode wave. In additional heating, the ERP and frequencies of the O-mode and X-mode are optional. Frolov et al. (1999, 2004) stated that additional X-mode heating suppresses the O-mode generation of high-frequency plasma turbulence in the form of suppression of the ponderomotive narrow con-

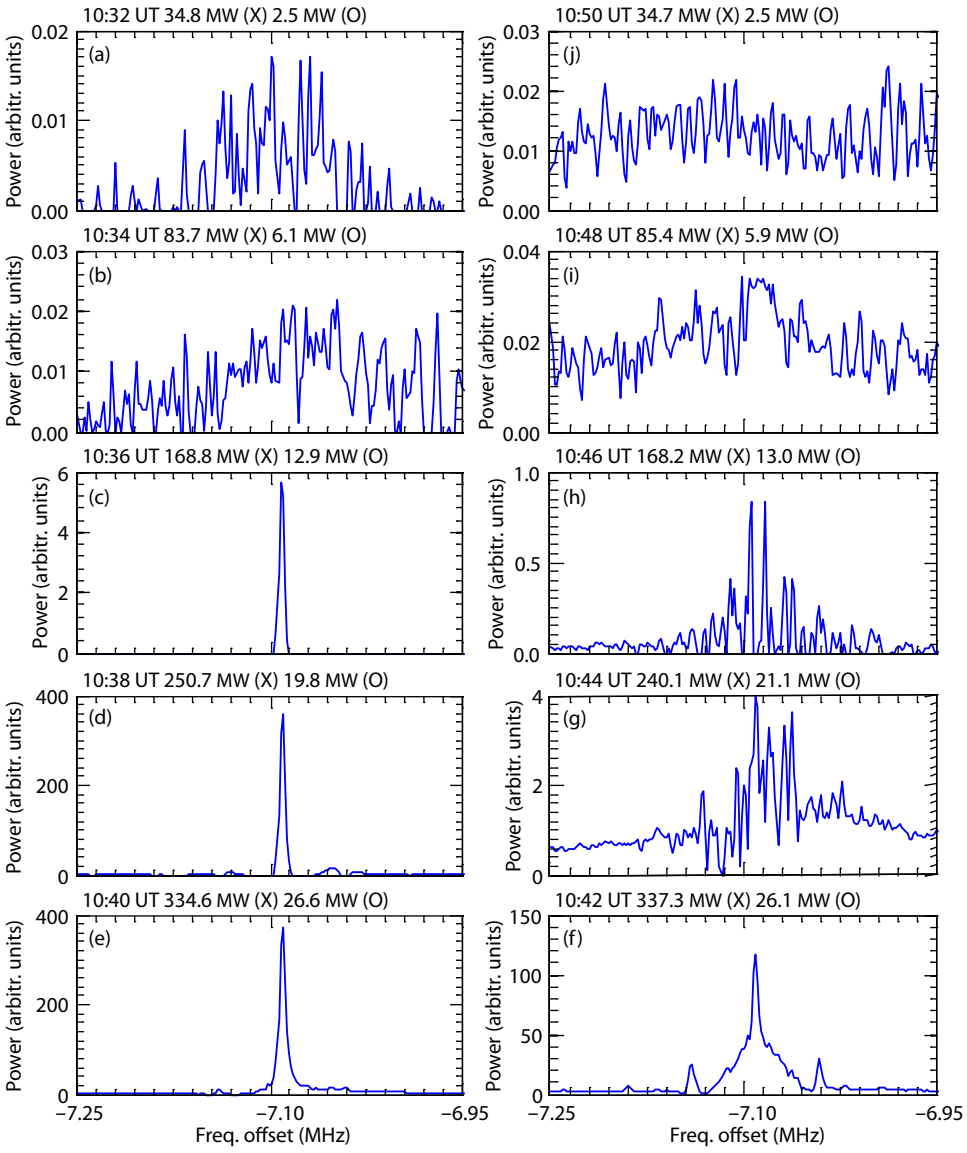

Figure 6. Plasma line spectra at a fixed altitude of 224.96 km with a pump wave frequency of f_0 = 7.1 MHz between 10:30 and 10:50 UT on October 30, 2015.

tinuum and downshifted maximum generation in SEE spectra. Gustavsson et al. (2009) presented the first observations of additional X-mode suppression of O-mode high-frequency-induced emission at 6,300 Å. In addition, Gustavsson et al. (2009) showed that by raising the heating of the background plasma, the additional X-mode suppresses the nonlinear process related to TPI driven by the O-mode. Another distinct difference between the experiment presented here and the additional heating experiments (Frolov et al., 1999; Gustavsson et al., 2009) is on the order of ERP. Frolov et al. (1999) reported that the ERPs of the O-mode and X-mode were 4–18 MW and 20–100 MW, respectively, whereas Gustavsson et al. (2009) observed that the ERPs of the two modes were 102 MW and 155 MW. In this work, however, we present the suppression of TPI in the presence of PDI and OTSI produced by the O-mode (2.5–26.6 MW) in X-mode (34.7–337.3 MW) heating. More experimental data are necessary to investigate the correlation between the suppression of TPI and ERP.

For further discussion, we propose a mechanism to explain the suppression of TPI caused by X-mode heating. X-mode heating causes electron temperature enhancements through ohmic heating, and the electric field threshold related to the growth rate of TPI depends on the electron temperature (Gustavsson et al., 2009; Blagoveshchenskaya et al., 2014). The relationship between the growth rate of TPI and the electron temperature is shown in the bottom panel of Figure 7, and the upper panel corresponds to the ERP as given in Figures 3a and 4a. We see that the electron temperature rises as the heating power increases. In the bottom panel, the blue dots are electron temperatures obtained from measurements in the UH resonance region, and the red dots are the growth rate of the TPI, which is calculated from equation (21) in Kuo (2014). The blue line and red line show the fit of the curves to the dots. The growth rates of the TPI and electron temperature are negatively correlated, and the correlation coefficient is −0.99, which can be seen from the blue and red lines. Therefore, we consider that the X-mode heating suppresses TPI by raising the elec-

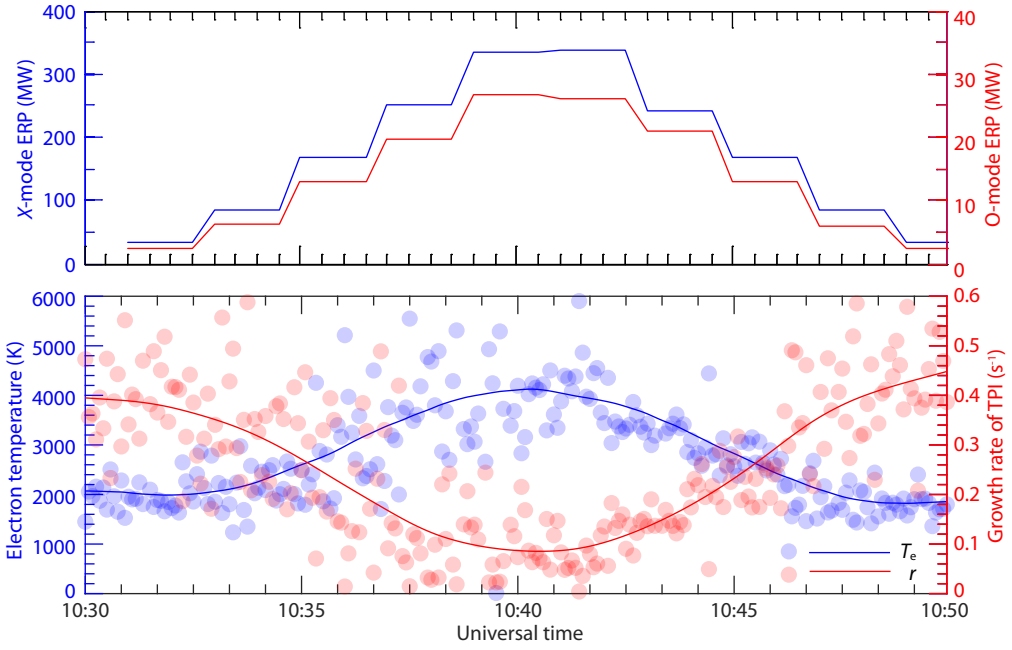

Figure 7. (upper panel) The ERP of X-mode (blue) and O-mode (red) pump waves during the entire cycle. (bottom panel) Electron temperatures obtained from measurements at the upper hybrid (UH) resonance region (blue dots), and growth rate of TPI calculated from the temperatures (red dots). The blue line and red line are the fit of the curves to the dots.

tron temperature, thereby allowing PDI to develop over a long time in the absence of TPI.

5. Summary

In cold-start O-mode heating, overshoot could be observed in the first experiment we showed. Overshoot occurred because the PDI was quenched after the FAIs related to TPI were fully established a few seconds after the pump was on. For comparison, we showed a second experiment with cold-start X-mode heating. Parametric decay instability occurred at the largest of the three pump wave powers and existed during the pump-on status instead of being quenched, as in the O-mode example. This result suggests TPI was suppressed by X-mode heating. The third experiment was a unique non-cold-start power-stepped X-mode heating. In this case, the HFILs and HFPLs were obtained at the O-mode reflection height, so we considered their generation as caused by leakage from the X-mode to the O-mode. For further confirmation, we analyzed the matching conditions of PDI and OTSI, which were stimulated by the O-mode and observed in the absence of TPI because PDI and TPI will compete. Further, in the third experiment, overshoot was not observed, so we concluded that TPI was inhibited by X-mode heating because of the increase in electron temperature. The negative correlation between the electron temperature and the growth rate of TPI supports this assumption.

Acknowledgments

EISCAT is an international scientific association supported by research organizations in China (China Research Institute of Radiowave Propagation (CRIRP)), Finland (Suomen Akatemia (SA)), Japan (National Institute of Polar Research (NIPR) and Solar-Terrestrial Environment Laboratory (STEL)), Norway (The Research Council of Norway (NFR)), Sweden (Swedish Research Council (VR)), and the United Kingdom (Natural Environment Research Council (NERC)). This work was supported by the National Natural Science Foundation of China (NSFC, grants 41204111, 41574146, 41774162, and 41704155) and the China Postdoctoral Science Foundation (grant 2017M622504). The experiment described in this work was carried out by the Russian team led by N. F. Blagoveshchenskaya. The data used in this research are available through the EISCAT Madrigal database (http://www.eiscat.se/madrigal/) and EISCAT Dynasonde database (https://dynserv.eiscat.uit.no/).

References

Blagoveshchenskaya, N. F., Borisova, T. D., Yeoman, T. K., Rietveld, M. T., Ivanova, I. M., and Baddeley, L. J. (2011). Artificial small-scale field-aligned irregularities in the high latitude F region of the ionosphere induced by an X-mode HF heater wave. *Geophys. Res. Lett.*, *38*(8), L08802. https://doi.org/10.1029/2011GL046724

Blagoveshchenskaya, N. F., Borisova, T. D., Yeoman, T. K., Rietveld, M. T., Häggström, I., and Ivanova, I. M. (2013). Plasma modifications induced by an X-mode HF heater wave in the high latitude F region of the ionosphere. *J. Atmos. Sol. Terr. Phys.*, *105-106*, 231–244. https://doi.org/10.1016/j.jastp.2012.10.001

Blagoveshchenskaya, N. F., Borisova, T. D., Kosch, M., Sergienko, T., Brändström, U., Yeoman, T. K., and Häggström, I. (2014). Optical and ionospheric phenomena at EISCAT under continuous *X*-mode HF pumping. *J. Geophys. Res. Space Phys.*, *119*(12), 10483–10498. https://doi.org/10.1002/2014JA020658

Blagoveshchenskaya, N. F., Borisova, T. D., Yeoman, T. K., Häggström, I., and Kalishin, A. S. (2015). Modification of the high latitude ionosphere F region by X-mode powerful HF radio waves: experimental results from multi-instrument diagnostics. *J. Atmos. Sol. Terr. Phys.*, *135*, 50–63. https://doi.org/10.1016/j.jastp.2015.10.009

Blagoveshchenskaya, N. F., Borisova, T. D., Kalishin, A. S., Yeoman, T. K., and

Häggström, I. (2017). First observations of electron gyro-harmonic effects under X-mode HF pumping the high latitude ionospheric F-region. *J. Atmos. Sol. Terr. Phys.*, *155*, 36–49. https://doi.org/10.1016/j.jastp.2017.02.003

Bryers, C. J., Kosch, M. J., Senior, A., Rietveld, M. T., and Yeoman, T. K. (2013). The thresholds of ionospheric plasma instabilities pumped by high-frequency radio waves at EISCAT. *J. Geophys. Res. Space Phys.*, *118*(11), 7472–7481. https://doi.org/10.1002/2013JA019429

Fejer, J. A. (1979). Ionospheric modification and parametric instabilities. *Rev. Geophys.*, *17*(1), 135–153. https://doi.org/10.1029/RG017i001p00135

Frolov, V. L., Kagan, L. M., Sergeev, E. N., Komrakov, G. P., Bernhardt, P. A., Goldstein, J. A., Wagner, L. S., Selcher, C. A., and Stubbe, P. (1999). Ionospheric observations of *F* region artificial plasma turbulence, modified by powerful X-mode radio waves. *J. Geophys. Res. Space Phys.*, *104*(A6), 12695–12704. https://doi.org/10.1029/1998JA900182

Frolov, V. L., Sergeev, E. N., Komrakov, G. P., Stubbe, P., Thidé, B., Waldenvik, M., Veszelei, E., and Leyser, T. B. (2004). Ponderomotive narrow continuum (NC_p) component in stimulated electromagnetic emission spectra. *J. Geophys. Res. Space Phys.*, *109*(A7), A07304. https://doi.org/10.1029/2001JA005063

Gustavsson, B., Newsome, R., Leyser, T. B., Kosch, M. J., Norin, L., McCarrick, M., Pedersen, T., and Watkins, B. J. (2009). First observations of X-mode suppression of O-mode HF enhancements at 6300 Å. *Geophys. Res. Lett.*, *36*(20), L20102. https://doi.org/10.1029/2009GL039421

Inhester, B., Das, A. C., and Fejer, J. A. (1981). Generation of small-scale field-aligned irregularities in ionospheric heating experiments. *J. Geophys. Res. Space Phys.*, *86*(A11), 9101–9106. https://doi.org/10.1029/JA086iA11p09101

Kuo, S. P., Lee, M. C., and Kossey, P. (1997). Excitation of oscillating two stream instability by upper hybrid pump waves in ionospheric heating experiments at Tromso. *Geophys. Res. Lett.*, *24*(23), 2969–2972. https://doi.org/10.1029/97GL03054

Kuo, S. P. (2014). Overview of ionospheric modification by High Frequency (HF) heaters-theory. *Prog. Electromagn. Res. B*, *60*, 141–155. https://doi.org/10.2528/PIERB14041805

Kuo, S. P. (2015). Ionospheric modifications in high frequency heating experiments. *Phys. Plasmas*, *22*(1), 012901. https://doi.org/10.1063/1.4905519

Lee, M. C., and Kuo, S. P. (1983). Excitation of upper-hybrid waves by a thermal parametric instability. *J. Plasma Phys.*, *30*(3), 463–478. https://doi.org/10.1017/S002237780000129X

Lehtinen, M. S., and Huuskonen, A. (1996). General incoherent scatter analysis and GUISDAP. *J. Atmos. Terr. Phys.*, *58*(1-4), 435–452. https://doi.org/10.1016/0021-9169(95)00047-X

Perkins, F. W., Oberman, C., and Valeo, E. J. (1974). Parametric instabilities and ionospheric modification. *J. Geophys. Res.*, *79*(10), 1478–1496. https://doi.org/10.1029/JA079i010p01478

Robinson, T. R. (1983). The heating of the high lattitude ionosphere by high power radio waves. *Phys. Rep.*, *179*(2-3), 79–209. https://doi.org/10.1016/0370-1573(89)90005-7

Senior, A., Rietveld, M. T., Häggström, I., and Kosch, M. J. (2013). Radio-induced incoherent scatter ion line enhancements with wide altitude extents in the high-latitude ionosphere. *Geophys. Res. Lett.*, *40*(9), 1669–1674. https://doi.org/10.1002/grl.50272

Showen, R. L., and Kim, D. M. (1978). Time variations of HF-induced plasma waves. *J. Geophys. Res. Space Phys.*, *83*(A2), 623–628. https://doi.org/10.1029/JA083iA02p00623

Stubbe, P., Kopka, H., Thidé, B., and Derblom, H. (1984). Stimulated electromagnetic emission: a new technique to study the parametric decay instability in the ionosphere. *J. Geophys. Res. Space Phys.*, *89*(A9), 7523–7536. https://doi.org/10.1029/JA089iA09p07523

Stubbe, P., Kohl, H., and Rietveld, M. T. (1992). Langmuir turbulence and ionospheric modification. *J. Geophys. Res. Space Phys.*, *97*(A5), 6285–6297. https://doi.org/10.1029/91JA03047

Stubbe, P. (1996). Review of ionospheric modification experiments at Tromsø. *J. Atmos. Terr. Phys.*, *58*(1-4), 349–368. https://doi.org/10.1016/0021-9169(95)00041-0

Thidé, B., Sergeev, E. N., Grach, S. M., Leyser, T. B., and Carozzi, T. D. (2005). Competition between Langmuir and upper-hybrid turbulence in a high-frequency-pumped ionosphere. *Phys. Rev. Lett.*, *95*(25), 255002. https://doi.org/10.1103/PhysRevLett.95.255002

Vas'kov, V. V., and Gurevich, A. V. (1975). Nonlinear resonant instability of a plasma in the field of an ordinary electromagnetic wave. *Zhurnal Eksperimentalnoi Teoreticheskoi Fiziki*, *69*, 176–188.

Vas'kov, V. V., and Ryabova, N. A. (1998). Parametric excitation of high frequency plasma oscillations in the ionosphere by a powerful extraordinary radio wave. *Adv. Space Res.*, *21*(5), 697–700. https://doi.org/10.1016/S0273-1177(97)01006-5

Wang, X., Cannon, P., Zhou, C., Honary, F., Ni, B. B., and Zhao, Z. Y. (2016a). A theoretical investigation on the parametric instability excited by X-mode polarized electromagnetic wave at Tromsø. *J. Geophys. Res. Space Phys.*, *121*(4), 3578–3591. https://doi.org/10.1002/2016JA022411

Wang, X., Zhou, C., Liu, M. R., Honary, F., Ni, B. B., and Zhao, Z. Y. (2016b). Parametric instability induced by *X*-mode wave heating at EISCAT. *J. Geophys. Res. Space Phys.*, *121*(10), 10536–10548. https://doi.org/10.1002/2016JA023070

Wang, X., and Zhou, C. (2017). Aspect dependence of Langmuir parametric instability excitation observed by EISCAT. *Geophys. Res. Lett.*, *44*(18), 9124–9133. https://doi.org/10.1002/2017GL074743